DOI: 10.1557/adv.2020.186

MRS Advances

Anisotropic Optical Properties of 2D Silicon Telluride

Romakanta Bhattarai,[1] Jiyang Chen,[1] Thang B. Hoang,[1] Jingbiao Cui,[2] and Xiao Shen[1]

[1]*Department of Physics and Materials Science, University of Memphis, Memphis, TN 38152, USA*

[2]*Department of Physics, University of North Texas, Denton, TX 76201, USA*

ABSTRACT

Silicon telluride (Si_2Te_3) is a silicon-based 2D chalcogenide with potential applications in optoelectronics. It has a unique crystal structure where Si atoms form Si-Si dimers to occupy the "metal" sites. In this paper, we report an ab initio computational study of its optical dielectric properties using the GW approximation and the Bethe-Salpeter equation (BSE). Strong in-plane optical anisotropy is discovered. The imaginary part of the dielectric constant in the direction parallel to the Si-Si dimers is found to be much lower than that perpendicular to the dimers. The optical measurement of the absorption spectra of 2D Si_2Te_3 nanoplates shows modulation of the absorption coefficient under 90-degree rotation, confirming the computational results. We show the optical anisotropy originates from the particular compositions of the wavefunctions in the valence and conduction bands. Because it is associated with the Si dimer orientation, the in-plane optical anisotropy can potentially be dynamically controlled by electrical field and strain, which may be useful for new device design. In addition, BSE calculations reduce GW quasiparticle band gap by 0.3 eV in bulk and 0.6 eV in monolayer, indicating a large excitonic effect in Si_2Te_3. Furthermore, including electron-hole interaction in bulk calculations significantly reduces the imaginary part of the dielectric constant in the out-of-plane direction, suggesting strong interlayer exciton effect in Si_2Te_3 multilayers.

INTRODUCTION

Since the last decade, two-dimensional materials have drawn a lot of interest in potential applications and fundamental sciences. Many 2D materials: graphene [1-3], transition-metal dichalcogenides such as MoS_2 [4], phosphorene [5,6], and more have been fabricated, and the investigations revealed interesting properties different from their bulk forms. Among the many properties of 2D materials, the optical properties are

particularity notable, as the low dimensionality significantly reduces dielectric screening, thus greatly enhancing the exciton binding energies [7]. As a result, 2D materials have attracted significant attention for optoelectronics. Moreover, in-plane optical anisotropy in 2D materials such as phosphorene [8], group IV mono-chalcogenides [9], ReS_2 [10], GaTe [11], and T_d WTe_2 [12] offers an additional degree of freedom for device design and have potentials in angle-dependent optical and optoelectronic applications [13,14]. It is also proposed that the dielectric anisotropy in two-dimensional SnO and SnSe monolayers can be utilized so that one can use a linearly polarized laser pulse to drive a phase transition in these materials [15].

Silicon telluride (Si_2Te_3) is a silicon-based layered material that is recently made into 2D multilayers[16]. This material has a peculiar crystal structure: the Si atoms form Si-Si dimers to fill 2/3 of the allowed "metal" sites between the Te layers [17, 18]. There are four possible orientations of each Si-Si dimers, three in-plane, and one out-of-plane. The rotation of a Si-Si dimer has an activation energy of 1 eV and can happen at room temperature [19]. The Si-Si dimer orientation adds an additional internal degree of freedom that is unique in this material. The optical properties of Si_2Te_3 have been experimentally investigated for potential applications in optoelectronics. Photoluminescence measurements show that the band gap emission was observed below 90 K, and the defect emission was observed at room temperature [20]. The relaxation of photocarriers also exhibits strong temperature dependence, possible related to the Si-Si dimer dynamics [21]. However, there are no theoretical calculations of the optical constants of Si_2Te_3 nor experimental measurement of the optical anisotropy. It was also demonstrated that the optoelectronic properties of the materials can be tuned by doping and intercalation [22]. For practical applications, Si_2Te_3 offers an additional advantage as it can be potentially compatible with the Si technology that is prevalent in the industry [16].

In this paper, we report a combined computational and experimental study of the optical properties of 2D Si_2Te_3. Using ab-initio many-body GW approximation and Bethe-Salpeter equation (BSE), we obtain the dielectric constants of bulk and monolayer of Si_2Te_3. The results show strong in-plane optical anisotropy in Si_2Te_3. The imaginary part of the dielectric constant in the direction parallel to the Si-Si dimers is significantly smaller than the value perpendicular to the dimer. This effect is due to the compositions of the valence and conduction bands. Experiments verify the existence of the optical anisotropy. Because the anisotropy is determined by the Si dimer orientation, it can potentially be dynamically controlled by electrical field and strain, which may be useful for new device design. We also find that including electron-hole interaction reduces the quasiparticle band gap by 0.3 eV in bulk and 0.6 eV in a monolayer, indicating a large excitonic effect in Si_2Te_3. In addition, including electron-hole interaction in bulk calculations significantly reduces the imaginary part of the dielectric constant in the out-of-plane direction, indicating strong interlayer excitons in this material.

THEORETICAL DETAILS

The calculations of the optical dielectric constants are carried out in three steps. In the first step, we perform standard density functional theory (DFT) calculations using the Perdew-Burke-Ernzerhof (PBE) exchange-correlation functional under generalized gradient approximation (GGA) [23]. The pseudopotential used throughout the calculation was constructed under the projected augmented wave (PAW) method [24]. The electronic convergence is achieved when the energy difference between two successive steps is less than 10^{-9} eV. The atomic positions are fully relaxed until the energy difference between two successive steps is less than 10^{-8} eV. The integration over the Brillouin zone was performed with a grid of 3×3×3 k-point grid centered at Γ. Static and

frequency-dependent dielectric constants are calculated by the DFT method, including the local field effect. In the second step, we carry out many-body calculations using the GW approximation [25,26] that includes the quasiparticle correction to the DFT Kohn-Sham states [27]. In the GW approximation, the electronic self-energy is approximated by a product of single-particle Green's function (G) and the screened Coulomb potential (W). In this work, single-shot GW (G_0W_0) calculations are performed. The calculation is done using 248 bands to take into account enough unoccupied bands. In the final step, we carry out calculations based on the Bethe-Salpeter equation (BSE) [28-30], which includes the electron-hole interaction (excitonic effect) that is absent in DFT and GW approaches. All the calculations were performed using the VASP (Vienna Ab initio Simulation Package) code [31].

The calculations are carried out for both bulk and monolayer of Si_2Te_3. Figure 1 shows the structural model of bulk Si_2Te_3 used in the calculations. This structure corresponds to the ground state of Si_2Te_3, where all the Si-Si dimers are oriented in the same direction to lower the total energy of the system [19]. Although Si_2Te_3, like many other 2D chalcogenides, has a hexagonal-like lattice due to the packing of Te atoms, the primitive unit cell of the ground state structure is actually triclinic because the two in-plane lattice vectors, a1 and a2, do not have the same length, as one of them is parallel to the Si-Si dimer and the other is not. Each bulk unit cell contains two vertically stacked monolayers. The primitive unit cell contains 8 Si atoms (4 Si-Si dimers) and 12 Te atoms. We choose the y-axis to be along the direction of the Si-Si dimer. The bulk Si_2Te_3 consists of a periodic repeating of such unit cell along the crystal axis in the out-of-plane direction.

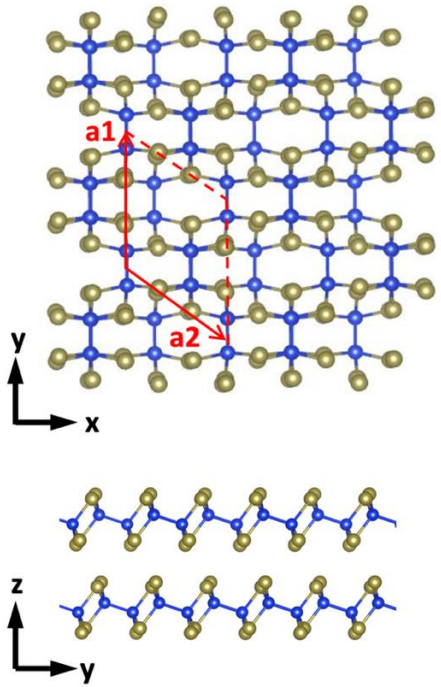

Figure 1. Top and side view of bulk Si_2Te_3. Si and Te atoms are in blue and tan color, respectively. The x- and y-axes are perpendicular and parallel to the Si dimers, respectively. The y-axis is aligned with the crystal axis a1.

EXPERIMENTAL DETAILS

Reflection measurements are introduced to probe the optical property of individual Si_2Te_3 nanoplates. The nanoplates were synthesized in a tube furnace (MTI 1200X) by using tellurium (30 mesh, 99.997%, Aldrich) and silicon powders (325 mesh, 99%, Aldrich) as source materials. Te and Si powders were placed in a ceramic crucible and loaded into the high-temperature tube furnace. Si substrate was placed downstream of the gas flow in a quartz tube. The substrate was kept at 652 °C while the source materials were heated to 850 °C during growth. High purity N_2 was used as the carrier gas with a flow rate of 20 sccm. The furnace was heated at a rate of 20 °C/min and maintained at 850 °C for Si_2Te_3 nanoplate growth for 5 min. After growth, the tube furnace was accelerated cool down to room temperature in 20 minutes by gradually opening the lid of the furnace.

The polarized reflection measurement was carried out at low temperature to reduce the thermal effect in the sample, i.e. the thermal quenching of the excitonic states. The sample was cooled down to 7 K in a vacuum chamber of an optical cryostat. In this measurement, the incident light source was from a Xenon arc lamp which produced a broad spectrum from 300 to 1000 nm. The non-polarized incident light was focused onto a single Si_2Te_3 nanoplate by a 20× objective lens. The polarized reflection spectrum was collected by the same objective lens and analysed by a linear polarizer (Thorlabs, LPVISC100-MP2), dispersed by a spectrometer (Horiba iHR550) and then detected by a charge-coupled-device.

THEORETICAL RESULTS

First, we calculate the static dielectric constants of Si_2Te_3 and check them against available experimental data obtained at room temperature. We need to note that a sample of Si_2Te_3 at the room temperature will contain a number of domains of Si-Si dimers in all three possible in-plane directions with equal possibility. Within each domain, there will be a large number of horizontally misaligned dimers and a small number (1%) of vertically misaligned dimers [19]. The measured dielectric constants at room temperature can be approximated by a mole-fraction average of all domains with different horizontal orientations. This average also takes into account the horizontally misaligned dimers within each domain, as they can be viewed as nanoscale domains themselves. Such an average is equivalent to taking the average value of ε_x and ε_y. The contributions from vertically misaligned dimers can be neglected since their population (mole-fraction) is small.

The static dielectric constants from DFT calculations are $\varepsilon_0(x) = 8.76$, $\varepsilon_0(y) = 7.19$, and $\varepsilon_0(z) = 6.17$. Taken an average of $\varepsilon_0(x)$ and $\varepsilon_0(y)$, we obtain the in-plane dielectric constant $\varepsilon_0(\perp) = 7.92$. This value, along with $\varepsilon_0(z) = 6.17$, are in agreement with the experimental values of $\varepsilon_0(\perp) = 8.5 \pm 0.2$ and $\varepsilon_0(\parallel) = 6.5 \pm 0.2$ [32]. It is interesting to note that the energy density in an electric field is $\frac{1}{2}\varepsilon E^2$, the ~20% difference between $\varepsilon_0(x)$ and $\varepsilon_0(y)$ suggests that the energy in an electric field is lower when it is applied along the Si-Si dimer direction. As Si-Si dimer rotation has an activation energy of 1 eV and thus can happen at room temperature, under strong electric field, the dimers may align with the applied electric field to reduce the energy of the field. Therefore, a large electrical field may be used as a method to control the dimer alignment and alter the resulting optical anisotropy, which is discussed below. In addition to electrical field, a mechanical strain can also promote the alignment of Si dimers and control the optical anisotropy.

Figure 2 shows the imaginary part of the frequency-dependent dielectric constants of bulk Si_2Te_3 from DFT, GW, and BSE methods. The electron energy loss function $\mathrm{Im}(-1/\varepsilon)$ from calculations agrees well with experiments and further confirms the validity of the model and the methods (see Supplemental Information). From the DFT calculations, we deduce a band gap of 1.45 eV. From the GW calculations, we find the quasi-particle band gap to be 2.24 eV, much higher than the DFT result. From the BSE calculations, we obtain an excitonic band gap of 1.95 eV. The results suggest that the exciton binding energy is about 0.3 eV in bulk Si_2Te_3. Figure 3 shows the results of monolayer Si_2Te_3. The quasi-particle band gap from GW calculation is 2.85 eV, which is higher than the bulk value. From the BSE calculations, we obtain an excitonic band gap of 2.24 eV, suggesting a large exciton binding energy of 0.6 eV in monolayer Si_2Te_3.

Strong anisotropy in the frequency-dependent dielectric constants is observed in both bulk and monolayer. From BSE calculations of bulk Si_2Te_3, the maximum $\mathrm{Im}(\varepsilon_x)$ is observed at 3.3 eV of photon energy, with a peak value of 13.0 (Figure 2a). Meanwhile, the maximum $\mathrm{Im}(\varepsilon_y)$ is observed at a similar photon energy, with a peak value of 8.5 (Figure 2b). The results indicate that Si_2Te_3 is highly anisotropy in the optical regime. The fact that $\mathrm{Im}(\varepsilon_x)$ is significantly larger than $\mathrm{Im}(\varepsilon_y)$ in optical regime is also observed in DFT and GW calculations, and in the case of 2D monolayers as well (Figure 3). The theoretical prediction of optical anisotropy is confirmed by the experimental results as described below.

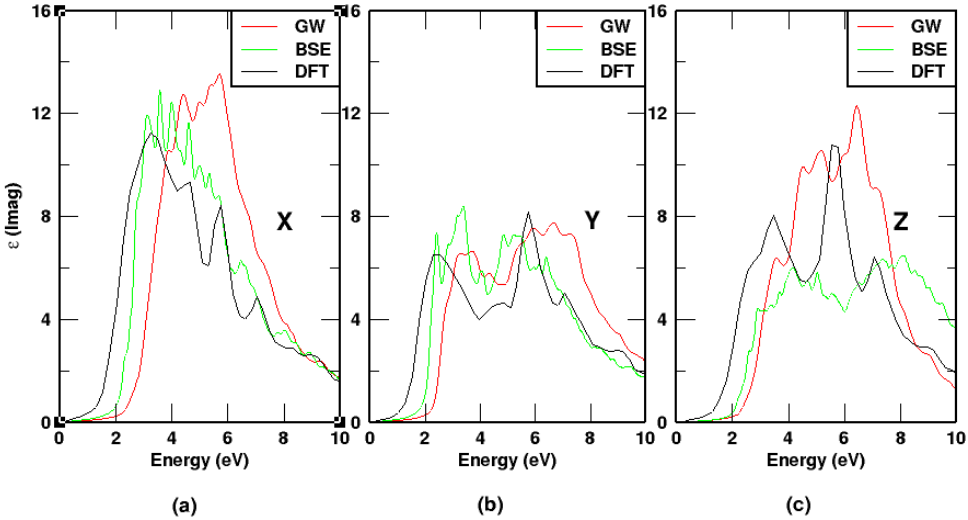

Figure 2. Imaginary part of the dielectric constant of bulk Si_2Te_3 along (a) x, (b) y, and (c) z-axes using three approaches (DFT, GW and BSE). The x- and y-axes are perpendicular and parallel to the Si dimers, respectively. The y-axis is aligned with the crystal axis a1.

EXPERIMENTAL RESULTS

A typical reflection spectrum of a single Si_2Te_3 nanoplate is shown in Figure 4a. The inset shows a scanning electron microscope image of the nanoplate. The reflection spectrum was normalized using the formula: $R = \frac{I_{pl} - I_{noise}}{I_{sub} - I_{noise}}$. Here I_{pl}, I_{sub} and I_{noise} are the reflection spectra from nanoplate, silicon substrate and camera noise. The reflection spectrum of a single Si_2Te_3 nanoplate shows two interesting features. First, below the

wavelength of 521 nm the normalized reflection value *R* was smaller than 1. This indicates that below the wavelength of 521 nm the incident photons were absorbed by the nanoplate. This observation hints an idea that the band gap of Si_2Te_3 nanoplate at 7 K is near 2.38 eV or 521 nm, and the photons above this energy will be absorbed. The inferred bandgap of 2.38 eV at 7 K in the Si_2Te_3 nanoplate is consistent with a previous reported value of 2.34 eV at 4.2 K for bulk Si_2Te_3 [32]. The absorbed photons then promote electrons from the valence band to the conduction band or other defect centres to form excitonic states, and these subsequently annihilate to emit photons. Secondly, above the wavelength 521 nm the normalized reflection value *R* was greater than 1, which indicates additional light was emitted from the nanoplate. It is very likely that the emitted light, such as photoluminescence resulted from the absorption at energy larger than the band gap and followed by a re-emission process. For instance, a high energy photon is absorbed to promote an electron to an excited state, which can then relaxed or scattered with defects or phonons before going back to the ground state and emit a photon at lower energy. This is consistent with previous observations that Si_2Te_3 has a complicated defect/surface states that can result in photoluminescence emission in the 600-900 nm range [20,21]. The intensity plot for each polarized reflection at 500 nm is shown in Figure 4b. The minimum intensities of reflection spectra at various polarizer angles show a cosine-like dependence. We observe the highest reflection at 22° and the lowest reflection at 112°, and the pattern is repeated by 180°. This result confirms an anisotropic optical absorption of Si_2Te_3, which is the result of the asymmetry in the dielectric constants.

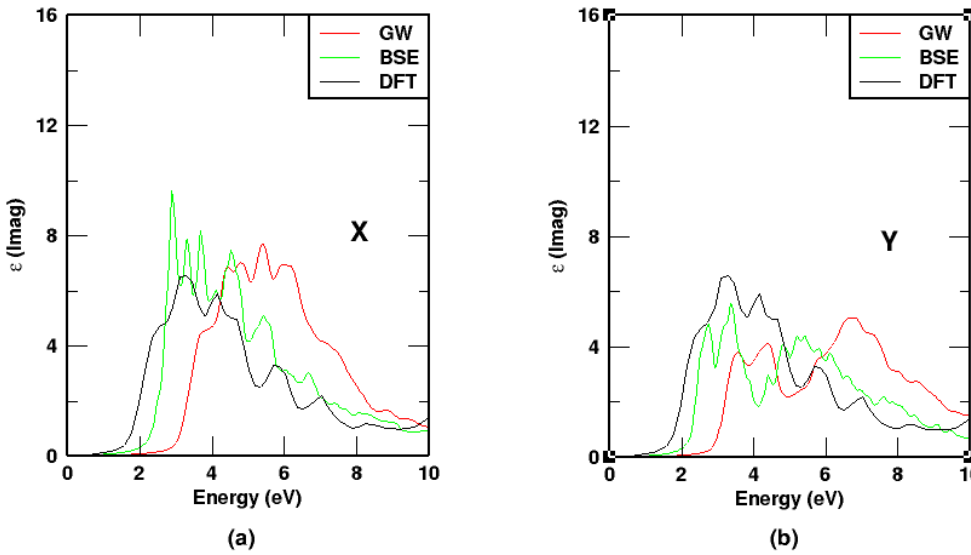

Figure 3. Imaginary part of the dielectric constant of monolayer Si_2Te_3 along (a) x, (b) y, axes using three approaches (DFT, GW and BSE). The x- and y-axis are perpendicular and parallel to the Si dimers, respectively.

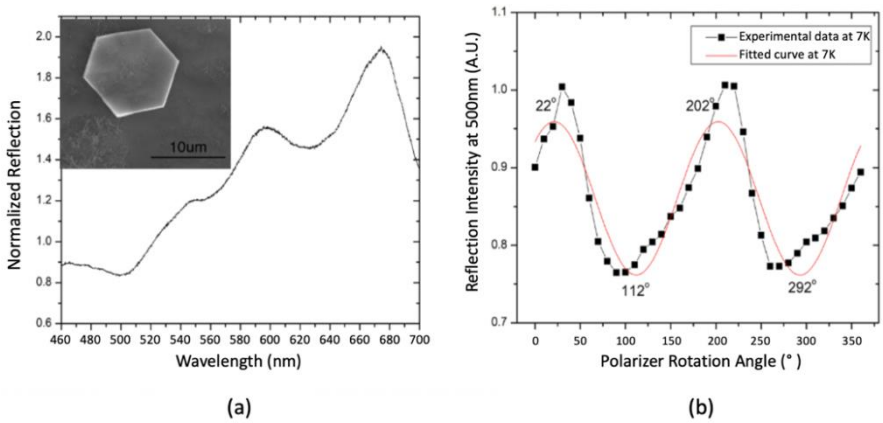

Figure 4. Reflection spectrum of a Si_2Te_3 nanoplate at 7 K (a) and the reflection intensity at different polarization angles from 0° to 360° (b). Inset of (a) is SEM image of the nanoplate.

DISCUSSION

The observed optical anisotropy in Si_2Te_3 can be understood from the specific composition of the conduction and valence bands. In Figure 5, we show the wave functions of the conduction band minimum (CBM) and valence band maximum (VBM) in bulk Si_2Te_3. The oscillation strength under electric field in x or y-direction is proportional to $\langle\phi_{CB}|x|\phi_{VB}\rangle$. As can be seen in Figure 5a, the VBM contains the Te 5p orbitals, one of which is marked as point 1. Meanwhile, for CBM (Figure 5c), the Si 2s orbitals are part of the wave function as marked as point 2 and 3. Under an electric dipole perturbation in the x-direction, this orbital at point 1 in VBM will expand horizontally and have a larger overlap with wave function at 2 and 3 CBM, resulting in a large oscillation strength. For electric dipole perturbation in the y-direction, the enhancement of the oscillation strength is not significant.

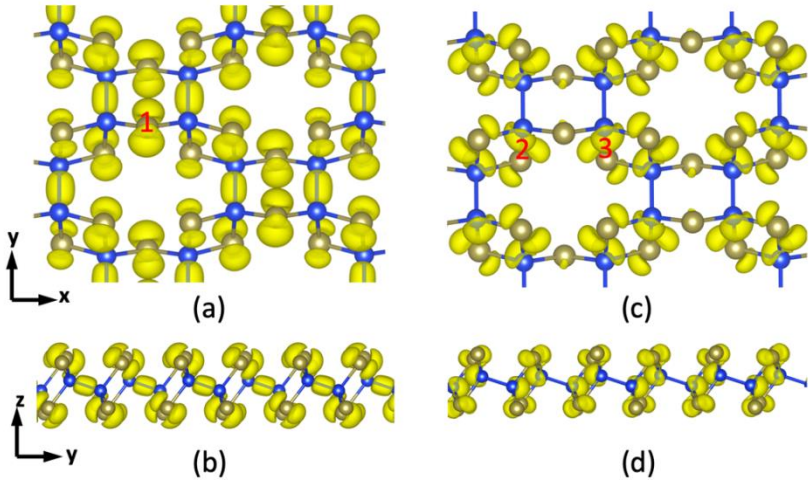

Figure 5. Top view (a) and side view (b) of the module-squared wavefunctions at VBM of bulk Si_2Te_3. Top view (c) and side view (d) of the module-squared wavefunctions at CBM. Each bulk unit cell contains two layers of Si_2Te_3, only one layer is shown here for clarity. The x- and y-axes are perpendicular and parallel to the Si dimers, respectively. The y-axis is aligned with the crystal axis a1.

Figure 2c shows an additional intriguing feature: the imaginary part of the dielectric constant in the vertical direction, $\mathrm{Im}(\varepsilon_z)$, is significantly smaller in BSE calculations than in DFT and GW calculations. This result indicates that the electron-hole interaction has a strong effect on the spectra of the quasi-electron and the quasi-hole when their wavevectors differ in the z-direction, which suggests a strong interlayer excitonic effect [33,34] in the optical properties of Si_2Te_3 multilayers. The strong interlayer excitonic effect can be understood from the particular compositions of the wave functions at the CBM and VBM as well. As shown in Figure 5, the VBM consists of Te 5p orbitals and the bonding orbitals of Si atoms, while the CBM of Si_2Te_3 consists of the Te 5p orbitals and the anti-bonding orbitals on Si atoms. From the side views of the wave functions (Figure 5b and 5d), it is obvious that both CBM and VBM contain Te 5p orbitals that extend into the space between the Si_2Te_3 layers. Therefore, the wave function of an electron in one layer and that of a hole in an adjacent layer can be closely spaced. The close proximity leads to large Coulombic interactions and naturally strong interlayer excitonic effect.

CONCLUSIONS

In this paper we report a combined computational and experimental study of the optical dielectric properties of Si_2Te_3. Computational results from the GW and BSE approaches suggest that the material exhibits strong optical anisotropy. The imaginary part of the dielectric constant in the direction parallel to the Si-Si dimers is much smaller compared to the direction perpendicular to the dimer. The anisotropy is verified by experimental data. The optical anisotropy can potentially be dynamically controlled by electric field or strain, which may be useful for applications. The electron-hole interaction reduces the quasiparticle band gap by 0.3 eV in bulk and 0.6 eV in the case of a monolayer, indicating a large excitonic effect in Si_2Te_3. Besides, BSE calculation significantly reduces the imaginary part of the dielectric constant of bulk Si_2Te_3 in the out-of-plane direction, suggesting a strong Coulombic interaction in the case of interlayer excitons.

ACKNOWLEDGMENT

This work was supported by National Science Foundation grant # DMR 1709528 and by the Ralph E. Powe Jr. Faculty Enhancement Awards from Oak Ridge Associated Universities (ORAU). Computational recourses were provided by University of Memphis High-Performance Computing Center (HPCC) and by the NSF XSEDE under grants # TG-DMR 170064 and 170076. TBH acknowledges a financial support from the Data Science research cluster of the FedEx Institute of Technology, the University of Memphis. We thank Dr. Li Yang for helpful discussion.

REFERENCES

[1] C. Berger, Z. Song, T. Li, X. Li, A. Y. Ogbazghi, R. Feng, Z. Dai, A. N. Marchenkov, E. H. Conrad, P. N. First, and W. A. De Heer, *J. Phys. Chem. B* **108**, 19912 (2004).
[2] K. S. Novoselov, A. K. Geim, S. V. Morozov, D. Jiang, Y. Zhang, S. V. Dubonos, I. V. Grigorieva, and A. A. Firsov, *Science* **306**, 666 (2004).
[3] Y. Zhang, Y. W. Tan, H. L. Stormer, and P. Kim, *Nature* **438**, 201 (2005).

[4] K. F. Mak, C. Lee, J. Hone, J. Shan, and T. F. Heinz, *Phys. Rev. Lett.* **105**, 136805 (2010).
[5] H. Liu, A. T. Neal, Z. Zhu, Z. Luo, X. Xu, D. Tománek, and P. D. Ye, *ACS Nano* **8**, 4033 (2014).
[6] M. Buscema, D. J. Groenendijk, S. I. Blanter, G. A. Steele, H. S. Van Der Zant, and A. Castellanos-Gomez, *Nano Lett.* **14**, 3347 (2014).
[7] P. Cudazzo, I. V. Tokatly, and A. Rubio, *Phys. Rev. B* **84**, 085406 (2011).
[8] N. Mao, J. Tang, L. Xie, J. Wu, B. Han, J. Lin, S. Deng, Wei Ji, Hua Xu, Kaihui Liu, Lianming Tong, and Jin Zhang, *J. Am. Chem. Soc.* **138**, 300 (2015).
[9] L. Huang, F. Wu, and J. Li, *J. Chem. Phys.* **144**, 114708 (2016).
[10] E. Zhang, P. Wang, Z. Li, H. F. Wang, C. Y. Song, C. Huang, Z.-G. Chen, L. Yang, K. T. Zhang, S. H. Lu, W. Y. Wang, S. S. Liu, H. H. Fang, X. H. Zhou, H. G. Yan, J. Zou, X. G. Wan, W. D. Hu, P. Zhou, and F. X. Xiu, *ACS Nano* **10**, 8067 (2016).
[11] S. Huang, Y. Tatsumi, X. Ling, H. Guo, Z. Wang, G. Watson, A. A. Puretzky, D. B. Geohegan, J. Kong, J. Li, T. Yang, R. Saito, and M. S. Dresselhaus, *ACS Nano* **10**, 8964 (2016).
[12] Q. J. Song, X. C. Pan, H. F. Wang, K. Zhang, Q. H. Tan, P. Li, Yi. Wan, Y. L. Wang, X. L. Xu, M. L. Lin, X. G. Wan, F. Q. Song, and L. Dai, *Sci. Rep.* **6**, 29254 (2016).
[13] H. Yuan, X. Liu, F. Afshinmanesh, W. Li, G. Xu, J. Sun, B. Lian, A. G. Curto, G. Ye, Y. Hikita, Z. Shen, S.-C. Zhang, X. Chen, M. Brongersma, H. Y. Hwang, and Y. Cui, *Nat. Nanotechnol.* **10**, 707 (2015).
[14] D. Li, H. Jussila, L. Karvonen, G. Ye, H. Lipsanen, X. Chen, and Z. Sun, *Sci. Rep.* **5**, 15899 (2015).
[15] J. Zhou, H. Xu, Y. Li, R. Jaramillo, and J. Li, *Nano Lett.* **18**, 7794 (2018).
[16] S. Keuleyan, M. Wang, F. R. Chung, J. Commons, and K. J. Koski, *Nano Letters* **15**, 2285 (2015).
[17] K. Ploog, W. Stetter, A. Nowitzki, and E. Schönherr, *Mater. Res. Bull.* **11**, 1147 (1976).
[18] P. E. Gregoriades, G. L. Bleris and J. Stoemenos, *Acta Crystallogr. Sect. B* **39**, 421 (1983).
[19] X. Shen, Y. S. Puzyrev, C. Combs, and S. T. Pantelides, *Appl. Phys. Lett.* **109**, 113104 (2016).
[20] K. Wu, W. Sun, Y. Jiang, J. Chen, L. Li, C. Cao, S. Shi, X. Shen, and J. Cui, *J. Appl. Phys.* **122**, 075701 (2017).
[21] J. Chen, K. Wu, X. Shen, T. B. Hoang, and J. Cui, *J. Appl. Phys.* **125**, 024306 (2019).
[22] M. Wang, G. Lahti, D. Williams, and K. J. Koski, *ACS Nano* **12**, 6163 (2018).
[23] J. P. Perdew, K. Burke, and M. Ernzerhof, *Phys. Rev. Lett.* **77**, 3865 (1996).
[24] P. E. Blöchl, *Phys. Rev. B* **50**, 17953 (1994).
[25] L. Hedin, *Phys. Rev. A* **139**, 796 (1965).
[26] M. S. Hybertsen, and S. G. Louie, *Phys. Rev. B* **34**, 5390 (1986).
[27] G. Onida, L. Reining, and A. Rubio, *Rev. Mod. Phys.* **74**, 601 (2002).
[28] E. E. Salpeter, and H. A. Bethe, *Phys. Rev.* **84**, 1232 (1951).
[29] S. Albrecht, L. Reining, R. Del Sole, and G. Onida, *Phys. Rev. Lett.* **80**, 4510 (1998).
[30] M. Rohlfing, and S. G. Louie, *Phys. Rev. Lett.* **81**, 2312 (1998).
[31] G. Kresse and J Furthmüller, *Phys. Rev. B* **54**, 11169 (1996).
[32] U. Zwick and K. H. Rieder, *Z. Physik B* **25**, 319 (1976).
[33] F. Ceballos, M. Z. Bellus, H. Y. Chiu, and H. Zhao, *ACS Nano* **8**, 12717 (2014).
[34] J. Horng, T. Stroucken, L. Zhang, E. Y. Paik, H. Deng, and S. W. Koch, *Phys. Rev. B* **97**, 241404 (2018).